Applied Geochemistry 39 (2013) 119–128

Contents lists available at ScienceDirect

Applied Geochemistry

journal homepage: www.elsevier.com/locate/apgeochem

Partitioning of Pb(II) during goethite and hematite crystallization: Implications for Pb transport in natural systems

Hong Phuc Vu *, Samuel Shaw [1], Loredana Brinza [2], Liane G. Benning

School of Earth and Environment, University of Leeds, Leeds LS2 9JT, UK

ARTICLE INFO

Article history:
Received 24 December 2012
Accepted 2 October 2013
Available online 10 October 2013
Editorial handling by M. Kersten

ABSTRACT

The interaction (e.g., adsorption and incorporation) of Pb with iron(III) (oxyhydr)oxide minerals has a significant influence on its partitioning and transport in many natural systems (e.g., rivers). The incorporation of Pb during ferrihydrite crystallization to hematite and goethite at neutral and alkaline pH, in the presence and absence of sulphate $\left(SO_4^{2-}\right)$ has been studied using X-ray Absorption Spectroscopy (XAS), X-ray Powder Diffraction (XRD), electron microscopic techniques and chemical extraction procedures. The XRD data showed that hematite and goethite were the end-products of crystallization at pH 5, whereas goethite was the sole product at pH 13. The Pb partitioning data revealed that upon crystallization at pH 5, ~60% of the initially adsorbed Pb remained on the surface of the crystalline hematite/goethite, while ~20% became incorporated with the remaining ~20% released back into solution. Lead incorporation occurred primarily during the initial stage of ferrihydrite crystallization prior to hematite/goethite formation at pH 5. The presence of SO_4^{2-} at pH 5 had little influence on the partitioning of Pb or mineral phases formed. At pH 13, 52% of the adsorbed Pb was incorporated during crystallization to goethite. Lead incorporation into this phase occurred over the entire crystallization process with adsorbed Pb incorporated during goethite crystal growth. X-ray Absorption Spectroscopy and unit cell size data demonstrated that Pb did not replace Fe within the structure of hematite or goethite, but was incorporated into defects or nanopores within the iron (oxyhydr)oxides.

1. Introduction

Iron(III) (oxyhydr)oxide phases (e.g., ferrihydrite, goethite and hematite) are common in many natural and contaminated land environments (e.g., rivers and acid mine drainage systems), and play an important role in a number of industrial processes (e.g., ferric oxide-based water purification systems) (Cornell and Schwertmann, 2003; Hassellov and von der Kammer, 2008). These phases have the ability to sequester (via adsorption and incorporation) large quantities of dissolved ions, including Pb, due to their high surface areas (up to 100's m^2/g) and reactivity, which make them a key control on the geochemistry of many environmental systems (Cornell and Schwertmann, 2003). For example, Kaste et al. (2006) showed that atmospherically deposited Pb can be remobilized and transported on iron oxide particles within top-soils. Colloidal iron (oxyhydr)oxide particles have also been described as the main transport vector for Pb in rivers (e.g., Hassellov and von der Kammer, 2008), and a variety of toxic elements (e.g., As) in acid mine drainage systems (Hudson-Edwards et al., 1999; Kimball et al., 1995). However, the mechanism by which Pb becomes incorporated into specific iron (oxyhydr)oxide phases, and the factors which affect these processes (e.g., solution composition) are poorly understood.

Poorly-ordered nanoparticulate ferrihydrite ($5Fe_2O_3{\cdot}9H_2O$) is usually the first phase formed when iron (oxyhydr)oxides precipitate directly from solutions at near neutral pH. This phase is thermodynamically unstable and will transform to crystalline phases such as hematite (α-Fe_2O_3) or goethite (α-FeOOH) when suspended in solution. The mechanisms of transformation to hematite and goethite under various chemical conditions (e.g., pH) have been well documented (Davidson et al., 2008; Fischer and Schwertmann, 1975; Loan et al., 2008, 2006; Murray et al., 2009; Schwertmann and Murad, 1983; Schwertmann et al., 2004; Shaw et al., 2005; Vu et al., 2010). These studies show that goethite and hematite form from ferrihydrite via two different mechanisms. Hematite crystallizes via initial aggregation of ferrihydrite nanoparticles, followed by the crystallization within the individual aggregates to form hematite, whereas, goethite forms via the dissolution of ferrihydrite and re-precipitation of goethite crystals (Fischer and Schwertmann, 1975; Schwertmann and Murad,

* Corresponding author. Current address: School of Earth Sciences, University of Melbourne, Victoria 3010, Australia. Tel.: +61 3 9035 6769; fax: +61 3 8344 7761.
E-mail address: hong.vu@unimelb.edu.au (H.P. Vu).
[1] Current address: School of Earth, Atmospheric and Environmental Sciences, University of Manchester, Manchester M13 9PL, UK.
[2] Current address: Diamond Light Source Ltd., Didcot, Oxfordshire OX11 0DE, UK.

0883-2927/$ - see front matter Crown Copyright © 2013 Published by Elsevier Ltd. All rights reserved.
http://dx.doi.org/10.1016/j.apgeochem.2013.10.001

1983). The transformation rate and proportions of hematite and goethite in the crystalline end-products are strongly influenced by pH and temperature (e.g., Davidson et al., 2008; Vu et al., 2010). Generally, hematite is dominant at near neutral pH and high temperatures, whereas goethite is favoured at high and low pH, and lower temperatures (Schwertmann et al., 1999, 2004; Schwertmann and Murad, 1983). Furthermore, for both phases, increasing pH and temperature results in an increase in the crystallization rate (Davidson et al., 2008; Schwertmann and Murad, 1983; Schwertmann et al., 2004; Vu et al., 2010). Finally, the presence of various dissolved anions (e.g., SO_4^{2-}) have been shown to alter the transformation pathway and rate of crystallization (Baltpurvins et al., 1996, 1997; Jang et al., 2003; Lin et al., 2003). Specifically, the presence of SO_4^{2-} retards the rate of ferrihydrite crystallization, and favours the formation of hematite over goethite (Baltpurvins et al., 1996; Lin et al., 2003).

Lead has been shown to adsorb onto the surface of iron (oxyhydr)oxide phases via an inner sphere edge-sharing, bidentate complex (Bargar et al., 1997b; Ostergren et al., 2000a; Trivedi et al., 2003). In the presence of SO_4^{2-}, studies have reported enhanced trace metal (including Pb) adsorption to iron (oxyhydr)oxides via ternary complexes (Collins et al., 1999; Elzinga et al., 2001; Ostergren et al., 2000a; Swedlund et al., 2003). The fate of Pb during the crystallization of co-precipitated Pb-ferrihydrite has been investigated at low temperatures ($\leqslant$70 °C) and near neutral pH (Ford et al., 1997, 1999; Martinez and McBride, 1998a,b; Martinez et al., 1999). In these studies Pb-doped ferrihydrite transformed to a mixture of goethite, hematite and lepidocrocite (e.g., Ford et al., 1999). During the transformation, a significant proportion of the Pb is incorporated within the iron (oxyhydr)oxide, but is subsequently expelled back into solution during the latter stages of crystallization, with only 10% of the coprecipitated Pb remaining within the final end-product (Ford et al., 1997, 1999). However, none of these studies obtained monomineralic crystalline end-products and thus the mechanism of incorporation is unknown. Furthermore, the partitioning of Pb (i.e., dissolved, surface adsorbed or incorporated) during ferrihydrite crystallization, and how this relates to the crystallization mechanism, and end-products are not currently known. We have recently shown that during the hydrothermal (T = 160–240 °C) transformation of ferrihydrite to hematite at high pH (pH $\sim$ 13), $\sim$70% of Pb initially adsorbed to ferrihydrite became trapped during ferrihydrite aggregation prior to full crystallization of hematite. However, $\sim$10% of this Pb was then released during the latter stage of hematite crystallization (Vu et al., 2010). Finally, despite the prevalence of SO_4^{2-} in the environment (e.g., oceans and acid mine drainage systems), there are no systematic studies of the effect of this anion on Pb incorporation into iron (oxyhydr)oxide phases.

In summary, to understand the role of iron (oxyhydr)oxide minerals on the mobility of Pb in environmental systems, a quantitative understanding of the Pb incorporation mechanism during the crystallization of iron (oxyhydr)oxide phases, and the factors which control the amount of Pb incorporation, is required. In this study we have used controlled crystallization experiments to investigate (1) the fate of Pb adsorbed to ferrihydrite during the crystallization to hematite/goethite (pH 5) or goethite (pH 13), (2) the molecular-scale mechanism of Pb incorporation into these phases, and (3) the effect of SO_4^{2-} on the fate and uptake mechanism of Pb.

2. Material and methods

Ferrihydrite was synthesized following the procedure of Cornell and Schwertmann (2003) and characterized as described in Vu et al. (2010). The density of ferrihydrite within the slurry was determined from the weight loss of a known amount of slurry (in triplicate) upon drying at 50 °C for 24 h. Prior to use in adsorption and transformation experiments the ferrihydrite was stored at 4 °C for up to 5 days.

All adsorption experiments were conducted in 125 ml polyethylene bottles under open air conditions. Lead stock solutions (50 mM) were prepared by dissolving $Pb(NO_3)_2$ in 0.5 M HNO_3, and a SO_4^{2-} stock solution (750 mM) was prepared by dissolving Na_2SO_4 in deionised (DI) water. Ferrihydrite suspensions with adsorbed Pb or Pb and SO_4^{2-} were aged with the aim of crystalizing to predominantly hematite at pH 5 or goethite at pH 13 (more details below). To ensure undersaturated conditions with respect to any Pb phases, the speciation of Pb at the conditions of our experiments were modelled using Geochemist Workbench (Bethke, 2004; details in Supplementary material text and Fig. S1). Furthermore, using the approach of Langmuir (1997) we estimated the ferrihydrite adsorption capacity to ensure that the Pb concentration we used did not surpass the maximum adsorption capacity of our ferrihydrite. Surface coverage was 13.3% and Γ was 0.1 mmol Pb/1 g ferrihydrite (see Supplementary material text).

To prepare the pH 5 experiments, a slurry equivalent of 0.1 g ferrihydrite was equilibrated for 24 h with 100 ml of 0.1 M $NaNO_3$ solution titrated to pH 5 using 0.1 M HNO_3. After 24 h, Pb or Pb and SO_4^{2-} were added from the stock solutions to reach 0.1 mM Pb and 1.5 mM SO_4^{2-}. In experiments where both Pb and SO_4^{2-} were present, the Pb was added first and allowed to adsorb to the ferrihydrite prior to the addition of SO_4^{2-} to avoid formation of any $PbSO_4$ solid phases. Subsequently, after 30 min of equilibration, SO_4^{2-} was spiked into the slurries in two increments, with 3 h between the two additions. During the adsorption experiments, the suspensions were constantly stirred. Changes in pH caused by the addition of the Pb or SO_4^{2-} were corrected by addition of 1 M NaOH or 1 M HNO_3. After 24 h the adsorption was considered completed and the final pH was recorded and readjusted to 5, if required. The suspensions were then immediately used in the transformation experiments.

To prepare a batch of samples equilibrated at pH 13, a slurry equivalent of 0.1 g ferrihydrite was equilibrated with 100 ml of a 1 M NaOH and 0.1 M $NaNO_3$ solution with initial Pb concentration of 0.1 mM. A 30 min adsorption time was chosen in order to avoid transformation of ferrihydrite to goethite (this time was chosen after conducting test experiments of equilibrating ferrihydrite at pH 13.2 from 10 min to 55 min, see Supplementary material Fig. S2 and Vu et al., 2010). Following this equilibration the slurries were used in the crystallization experiments described below.

The transformation experiments at pH 5 were performed by aging the samples containing Pb or Pb and SO_4^{2-} adsorbed ferrihydrite slurry at 92 °C. Any loss due to evaporation was maintained by adding DI water (total changes in volumes were less than 5%). The pH was measured and readjusted daily to 5 using 0.1 M NaOH (pH of slurries always in range 4.5 to 5). After 2, 8, 24, 48, 72, 96 and 120 h, a sample was cooled and either used in desorption experiments (see below) or centrifuged for solid extraction and characterization. The resulting solids were either frozen immediately in liquid N_2 (for X-ray spectroscopic analysis) or washed thoroughly by DI water and freeze-dried (for analyses of the specific surface area, X-ray diffraction and electron microscopy). The supernatants were filtered using 0.2-μm cellulose acetate filters. One aliquot of the supernatants was used directly for SO_4^{2-} analysis while another was acidified to 0.5 M HNO_3 for Pb and Fe analysis. The crystallization of Pb adsorbed ferrihydrite at pH 13 was carried out and sampled as above, but with the experiments performed at room temperature ($\sim$21 °C). Experiments were conducted for 5 days and samples collected after 2, 8, 24, 48, 72, 96 and 120 h.

Chemical extractions were performed to quantify the speciation of Pb during the crystallization process using the procedure of Vu

et al. (2010). The mass balance of Pb in each experiment can be defined as the sum of Pb in solution (Pb-SL), surface adsorbed Pb (Pb-SF) and incorporated Pb (Pb-INC) via:

$$(\text{Pb-T}) = (\text{Pb-SL}) + (\text{Pb-SF}) + (\text{Pb-INC}) \quad (1)$$

where (Pb-T) is the total amount of Pb initially added into the system. Firstly, the proportion of Pb in solution was determined from the amount of Pb in the filtered supernatant of each sample. Secondly, an experimental suspension was titrated quickly to pH 2 using 1 M HNO_3 (pH 5 system) or 3 M HNO_3 (pH 13 system) and equilibrated for 30 min. This led to the desorption of Pb from the iron (oxyhydr)oxide surfaces (Ford et al., 1997; Kparmwang, 2003; Li et al., 2005). The stability of ferrihydrite, goethite and hematite at pH 2 were tested by equilibrating these minerals with a solution at pH 2 then monitoring dissolved Fe over time (Supplementary material, Fig. S9). In the ferrihydrite stability experiments the concentration of dissolved Fe after 30 min of equilibrium at pH 2 was 0.17 mM, corresponding to 1.5% of the total ferrihydrite, which is considered as a negligible amount. After desorption, the resulting solid and liquid samples were separated by centrifugation. The extracted solution contained Pb which was the sum of Pb in solution and surface adsorbed Pb. The surface bound Pb (Pb-SF) was calculated by subtracting Pb in solution (Pb-SL) from the amount of Pb extracted at pH 2 for 30 min. In addition, dissolved Fe in the extracted solutions was also quantified to determine if any iron (oxyhydr)oxide dissolved during the acid desorption process. Finally, the incorporated Pb (Pb-INC) was determined by mass balance from the difference between the Pb-T and Pb-SL + Pb-SF.

The solid materials from the synthesis, adsorption and crystallization experiments were characterized by X-ray Powder Diffraction (XRD, Philips PW1050 X-ray diffractometer, Cu Kα fitted with a post sample monochromator to remove the Fe fluorescence signal). Additional XRD data were collected from selected samples with a silicon internal standard present to ensure accurate 2θ calibration. These data were used to determine the unit cell dimension of the crystalline phases present within the samples. Unit cell dimensions for the crystalline end-products were calculated using the Unitcell software (Holland and Redfern, 1997). Rietveld analysis of the XRD data was carried out using Topas 4–2 (Bruker, 2009) to calculate the amount of ferrihydrite, hematite and goethite in all solid samples. The freeze-dried samples were imaged using a Field Emission Gun Scanning Electron Microscope (FEG-SEM, LEO1530, operated at 3 keV) and a FEG-Transmission Electron Microscope (FEG-TEM, Phillips, CM200, operated at 197 keV) fitted with an ultra-thin window energy dispersive X-ray (EDX) spectrometer (Oxford Instruments ISIS). BET surface area was measured using a Gemini V2365 system (Micromeritics Instrument Corp.).

X-ray absorption spectra (XAS) at the Pb-L_{III} edge (13,055 eV) were collected at station 16.5 of the Synchrotron Radiation Source (SRS), Daresbury Laboratory, United Kingdom. Various samples were analyzed including the Pb adsorbed ferrihydrite starting materials, reaction end-products and end-product samples with surface Pb removed by desorption at pH 2. All experimental samples were analyzed using a liquid nitrogen cryostat with the samples at 77 K. The absorption edge spectra were aligned at 13,055 eV using Pb metal foil, and collected in fluorescence mode using a 30-element Ge solid-state detector. XAS spectra of the following minerals or chemical reagent: anglesite ($PbSO_4$), plattnerite (PbO_2), lanarkite ($Pb_2(SO_4)O$), cerussite ($PbCO_3$), PbO and $Pb(NO_3)_2$ were collected as Pb standards in transmission mode. All XAS data was fitted using the EXCURV98 software (Binsted, 1998) to extract the coordination numbers, bonding distances and atom types to the nearest neighbour atoms surrounding the central atom (Pb). The Debye Waller factors ($2\sigma^2$) were initially unconstrained when fitting the EXAFS data. Initial fitting suggested that the Debye Waller factors for most shells were close to 0.02 Å^2. The Debye Waller factors were then fixed at 0.02 Å^2 for all shells to reduce the number of variable in each fits, and to ensure consistent fitting between the datasets.

The aqueous concentration of Pb was quantified by atomic absorption spectrometry (AAS) using a Varian AAS-10 spectrometer. Sulphate was analyzed by ion chromatography using a Dionex DX-600 with an EDS50A UVD 17OU detector, an Ionpac AS16 column, a GS50 gradient pump and an AS50 autosampler. Finally, aqueous Fe concentrations were analyzed by the ferrozine method (Viollier et al., 2000) using a Cecil CE 3041 UV/VIS spectrophotometer. All reported errors for the solution analyses represented standard deviation from duplicate experiments or of two repeated experiments.

3. Result and discussion

3.1. Transformation of ferrihydrite at pH 5 and 13

The XRD data showed that in all pH 5 experiments ferrihydrite crystallized to a mixture of hematite and goethite (Fig. 1 and Supplementary material Fig. S3 and Table S1). The crystallization occurred in two stages, with stage one (0–8 h) being characterized by the presence of ferrihydrite as evidenced by two broad XRD peaks typical of 2-line ferrihydrite. In stage two, both goethite and hematite crystallized with the broad peaks for ferrihydrite absent from the XRD patterns at the end of the experiment (96 h).

Photomicrographs of the crystalline end-products (96 h) confirmed hematite and goethite as the phases present (Fig. 2, and Supplementary material Fig. S6a–c). Hematite was present as 30–120 nm rhombohedral crystals, while goethite consisted of needle-like crystals 50–200 nm in length. The corresponding TEM-EDX analyses revealed that Pb was associated with both phases (insets in Fig. 2, and Supplementary material Fig. S7).

The formation of a mixture of hematite and goethite is contrary to a similar study where the pure hematite crystallization was observed at 92 °C and pH 6.5 (Combes et al., 1990). However, Combes et al. (1990) used a ferrihydrite gel that was crystalized without the removal of the original electrolyte following ferrihydrite synthesis. The presence of other ions (e.g., Na^+ and NO_3^-) would have increased the ionic strength of the background electrolyte, which is known to favour hematite formation over goethite (Cornell and Giovanoli, 1985; Schwertmann et al., 1999). In addition, the difference in pH also contributed to the difference in mineral content in the end-products. Combes et al. (1990) conducted transformation experiments at pH 6.5 which favours the formation of hematite,

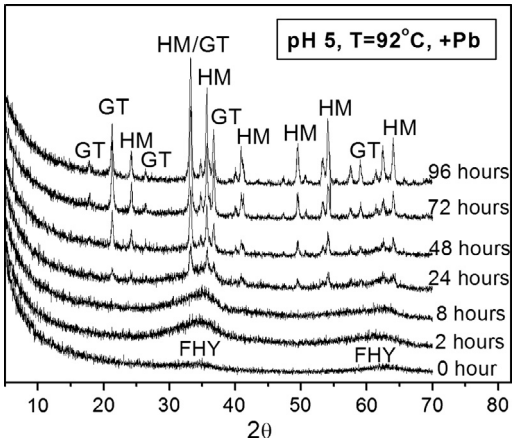

Fig. 1. X-ray Powder Diffraction patterns from solid phases during the crystallization of ferrihydrite with Pb at 92 °C and pH 5, in the absence of SO_4^{2-}. FHY = ferrihydrite, GT = goethite and HM = hematite.

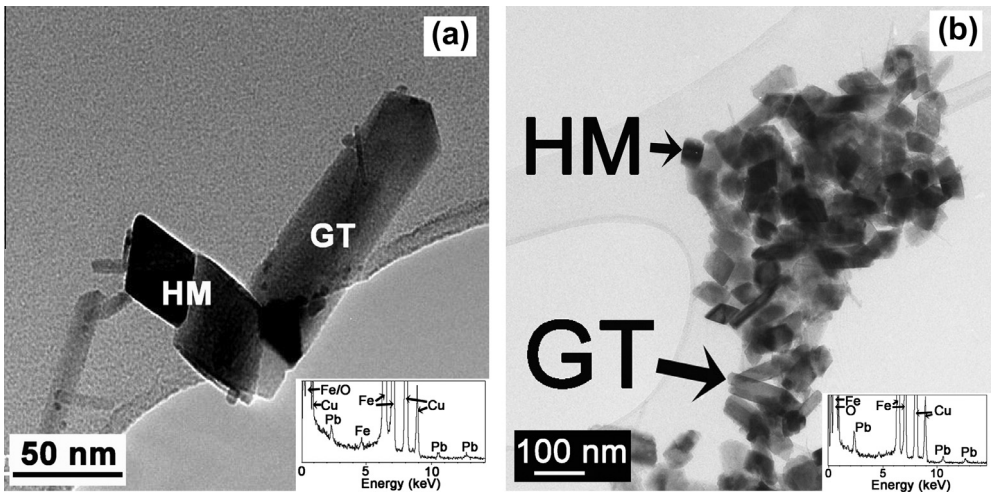

Fig. 2. Transmission Electron Microscope (TEM) images of reaction end products after 96 h (GT = goethite and HM = hematite) from the ferrihydrite crystallization experiments at pH 5 and 92 °C in the (a) presence of Pb and absence of SO_4^{2-}, (b) the presence of Pb and SO_4^{2-}. Inset TEM-EDX spectra showing that Pb was associated with hematite/goethite end-product (the presence of Cu in the spectra is due to the TEM grids).

while our transformation experiments were conducted at pH 5 thus a mixture of hematite and goethite was formed.

The proportions of ferrihydrite, goethite and hematite with time during the transformations at pH 5 as determined by Rietveld analysis are presented in Fig. 3, Supporting material Fig. S5 and Tables S1. A linear relationship between log (amount of ferrihydrite in sample) and time (Supporting material Fig. S4) suggested that the transformation of ferrihydrite at pH 5 was a first-order reaction, which is consistent with previous studies of the transformation of ferrihydrite (Baltpurvins et al., 1996; Lin et al., 2003; Schwertmann and Murad, 1983). Rietveld analysis indicates that the end products of the reaction are 53–55% hematite and 44–38% goethite with 3–7% residual ferrihydrite (Table S1), with little effect of SO_4^{2-} on the proportion of hematite vs. goethite crystallized.

In contrast, at pH 13 and ambient temperatures, the XRD data showed that in the presence of Pb, ferrihydrite crystallized to goethite only (Fig. 4 and Supplementary material Table S2). In these transformation experiments, an induction period (⩽2 h) was followed by the crystallization of goethite (Table S2) which was complete by 24 h. The formation of goethite in our experiments (at pH 13 and room temperature) is consistent with previous studies at low temperatures and alkaline conditions, which showed that goethite was the stable end-product of ferrihydrite crystallization under these conditions (Cornell and Giovanoli, 1985; Schwertmann and Murad, 1983; Schwertmann et al., 2004).

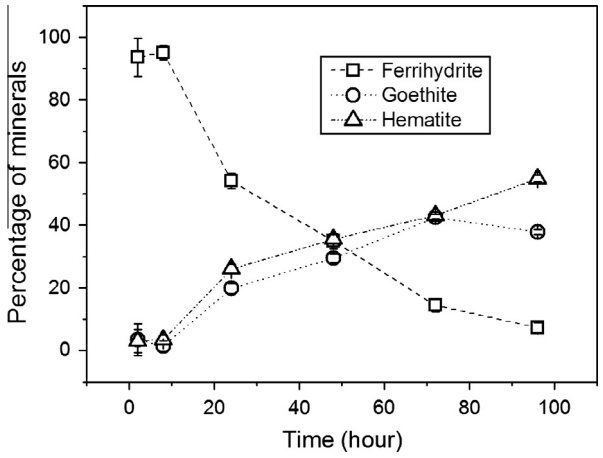

Fig. 3. The proportion of ferrihydrite, goethite and hematite with time from the experiment at pH 5 and 92 °C in the presence of Pb and the absence of SO_4^{2-}.

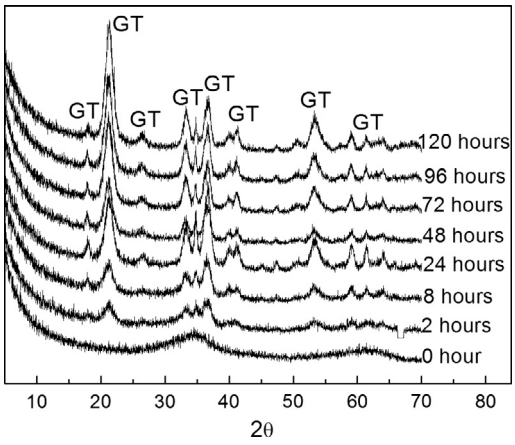

Fig. 4. X-ray Powder Diffraction patterns from the crystallization of ferrihydrite with adsorbed Pb at pH 13 (GT = goethite).

Imaging of the end-product materials confirmed needle-like goethite crystals 50–150 nm in length, as the sole reaction product (Fig. 5 and Supplementary material Fig. S6d). The goethite crystals were noticeably thinner than the goethite observed in the pH 5 and 92 °C experiments (Fig. 2). Also, TEM-EDX analyses indicated that Pb was associated with the goethite (Fig. 5, inset).

3.2. The fate of Pb during hematite and goethite crystallization

3.2.1. Pb partitioning during ferrihydrite transformation at pH 5 and 92 °C

The Pb speciation data (Fig. 6, Supplementary material Fig. S8 and Table S3) showed that during ferrihydrite crystallization at pH 5 Pb partitioning changed via a two-stage process, reflecting the two-stages of crystallization at pH 5. In addition, the presence of SO_4^{2-} did not significantly affect the Pb partitioning during crystallization. The first stage (between 0 to 8 h) coincided with the period prior to the initiation of crystallization (Fig. 1), while the second stage (from 8 h to the end of the experiments) overlapped

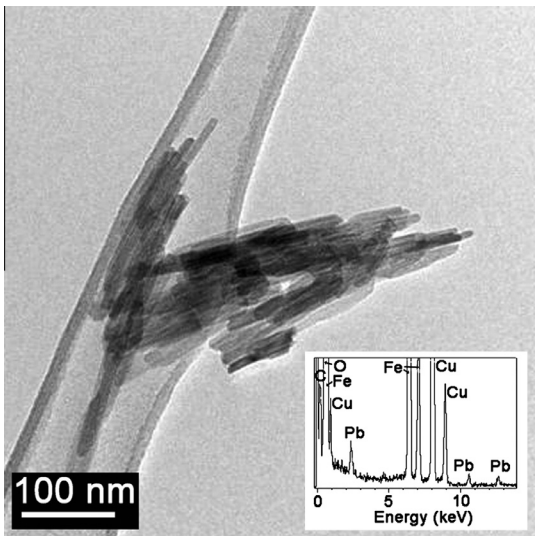

Fig. 5. Photomicrograph of goethite formed from ferrihydrite crystallized at pH 13 for 120 h in the presence of Pb, and corresponding TEM-EDX spectra (inset).

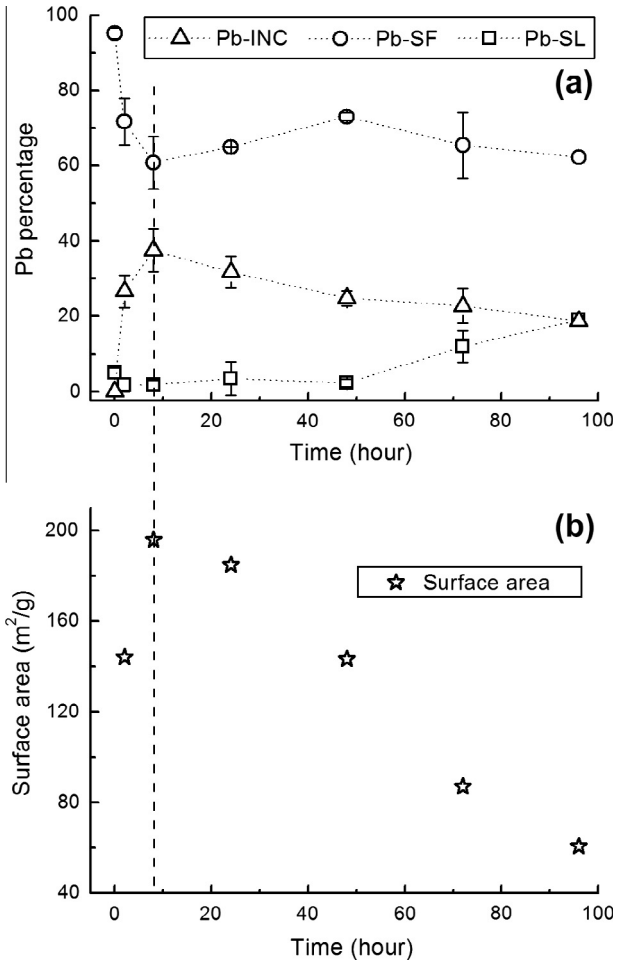

Fig. 6. (a) Partitioning of Pb during ferrihydrite crystallization at pH 5 and 92 °C, in the presence of Pb and the absence of SO_4^{2-}, (b) corresponding changes in the surface area of the solid phases. The dashed vertical line separates the first and the second stage of Pb partitioning. Pb-SL = Pb in solution, Pb-SF = surface adsorbed Pb and Pb-INC = incorporated Pb.

with the formation of hematite and goethite. At the beginning of the experiments (0 h, Fig. 6 and Supplementary material Fig. S8) Pb was fully adsorbed onto the starting ferrihydrite. During stage one, a sharp increase in the proportion of Pb incorporated into the solids (from 0% to ~30%) occurred, which was mirrored by a corresponding decrease in the surface bound Pb (from 100% to ~70%). The dissolved Pb remained relatively unchanged during stage 1. Concomitantly, the surface area of the solids was high, and in the SO_4^{2-} system the aqueous SO_4^{2-} concentration increased significantly during stage one (Figs. 6 and 7 and Supplementary material Fig. S8).

In the second stage (>8 h), the crystallization of hematite and goethite was coincident with a decline in the proportion of incorporated Pb (from ~30% to ~20%) and a dramatic decline in the surface area of the solids (from ~210 m^2/g to ~50 m^2/g, Fig. 6, Supplementary material Fig. S8 and Table S3). During this stage the dissolved Pb increased gradually from 1% to 18%, whereas the adsorbed Pb decreased slightly, from ~70% to ~60%. In the presence of SO_4^{2-} during the second stage, the aqueous SO_4^{2-} concentration continued to rise from 63% to 78% and then levelled off (Fig. 7) indicating that most of the SO_4^{2-} returned to the solution during crystallization. It should be noted that small amounts of dissolved Fe were detected in the desorption solutions (i.e., in samples taken at 2, 8 and 24 h), which equated to dissolution of <3.0% of the total ferrihydrite in the system. The partitioning of Pb data was thus considered unaffected by this dissolution during desorption.

Vu et al. (2010) observed a similar Pb uptake process for hematite formed at pH 13 and high temperature (160–240 °C) and suggested that Pb incorporation was controlled by aggregation of ferrihydrite nanoparticles occurring prior to hematite crystallization, which trapped the adsorbed Pb ions within the aggregates. Our results are partially consistent with this, and we suggest that Pb is incorporated rapidly during the very early stages of crystallization prior the formation of significant amounts of crystalline material. If the Pb is trapped due to aggregation of ferrihydrite, a decrease in surface area of the solid phases would be expected during this phase of the reaction (Vu et al., 2010), however we observe an increase. The reason for this increase in surface area during the early stages of the reaction is unclear. Potentially, the observed increase may be due to errors associated with the BET measurement of these high surface area materials. Alternatively, the decrease in pH from 5 to 4.5 observed during the early stages of this experiment or reduction in ionic strength due to the sample washing in DI water may have caused disaggregation and an increase in the surface area of the iron (oxyhydr)oxide samples (Cornell and Schwertmann, 2003; Yuwono et al., 2012).

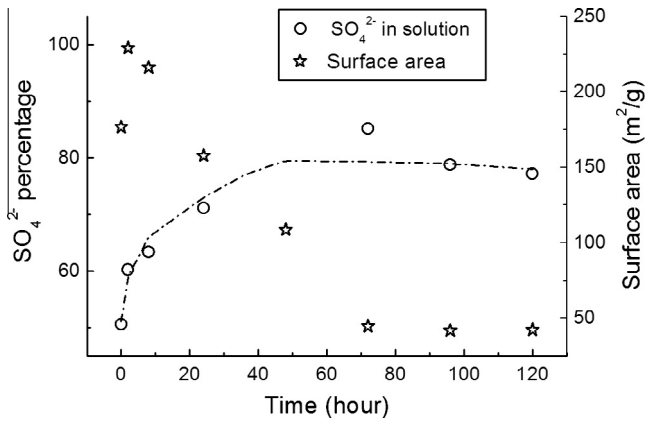

Fig. 7. Concentration of SO_4^{2-} in the supernatant solution during ferrihydrite crystallization at pH 5 and 92 °C in the presence of Pb and SO_4^{2-}, and the surface area of solid phases. The dashed vertical line separates the first and the second stage of Pb partitioning.

The second stage of the crystallization reaction at pH 5, where the ferrihydrite crystallized to hematite and goethite (Figs. 1 and 6, S3 and S8), was associated with the release of the incorporated Pb into solution. Previous studies of hydrothermal hematite crystallization at pH 13 (Vu et al., 2010) have suggested that Pb incorporated into defect sites during the initial ferrihydrite aggregation, and was rejected during crystallization to hematite. Our results from ferrihydrite crystallization at pH 5 are consistent with this idea as approximately 10% of the Pb originally incorporated into the iron (oxyhydr)oxides during stage one was released into the solution as the hematite and goethite crystallized. However, it should be noted that during the final stages of the reaction (72–96 h) there was a small increase in the amount of hematite relative to goethite. This suggests that, although the crystallization of ferrihydrite is complete, the system may not be at equilibrium and with further aging all the goethite may transform to hematite. This in turn may lead to a further release of Pb from the solid phase.

The presence of SO_4^{2-} slightly enhanced the amount of Pb incorporated into the final crystalline product at pH 5, but by less than 5% (Fig. 6 and Supplementary material Fig. S8). The surface area of the ferrihydrite used in the experiments with SO_4^{2-} was higher than in the pure Pb experiments, which may have led to slightly more Pb becoming trapped during particle aggregation. The difference in the surface area of the starting ferrihydrite in the experiments with and without sulphate is likely to be due to differences in the batches of ferrihydrite syntheses for these two sets of experiments and/or error of BET analysis, which can be up to 20 m^2/g. Previous studies have shown that SO_4^{2-} promoted the adsorption of Pb on the surface of iron (oxyhydr)oxides (Elzinga et al., 2001; Ostergren et al., 2000a; Swedlund et al., 2003), which could potentially increase Pb uptake during crystallization. However, in our experiments the SO_4^{2-} was desorbed during transformation, which may explain why the increase in incorporated Pb was small. This is also consistent with Pb local environment derived from the EXAFS data (see below), which shows no difference between the system with and without SO_4^{2-}. The release of SO_4^{2-} during hematite crystallization is likely to be due to the decline in surface area of the solids in the system (Fig. 6 and Supplementary material Fig. S8), which led to a decline in the available surface sorption sites.

3.2.2. Pb partitioning during ferrihydrite transformation at pH 13 and 21 °C

The Pb partitioning data during the crystallization of ferrihydrite to goethite at high pH showed that all Pb was adsorbed to the ferrihydrite at the beginning of the reaction (0 h, Fig. 8). During the main phase of goethite crystallization (0–24 h, Fig. 8) there was a sharp increase in incorporated Pb from 0% to 45% and a corresponding decrease in adsorbed Pb (from 100% to 53%). Coincident with this increase in incorporated Pb was a significant decrease in the surface area of the solid phase (from 184 m^2/g to 124 m^2/g). Following goethite crystallization (after 24 h, Fig. 8) only minor changes in the Pb partitioning was observed with the slight decrease in adsorbed Pb from 53% to 45% being mirrored by a small increase in dissolved and incorporated Pb. During this stage, the surface area decreased further and levelled off around 110 m^2/g after 120 h (Fig. 8).

It should be noted that in the desorption experiments at pH 13, significant amounts of dissolved Fe were measured in the solution of the first two samples taken at 2 and 8 h. Calculations from the concentration of dissolved Fe suggested that 34% and 24% of the total ferrihydrite were dissolved from the 2 and 8 h samples, respectively. This may have led to an overestimation of the amount of adsorbed Pb, and correspondingly an underestimation of incorporated Pb, at these time points. Goethite is known to form from ferrihydrite via a dissolution/re-precipitation mechanism

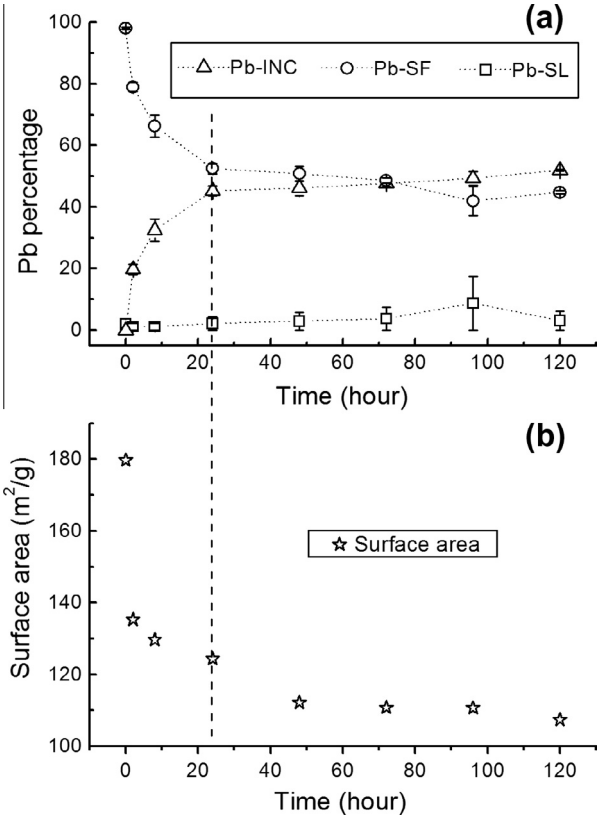

Fig. 8. (a) Partitioning of Pb during ferrihydrite crystallization at pH 13 in the presence of Pb and (b) corresponding changes in the surface area of solid phases. Pb-SL = Pb in solution, Pb-SF = surface adsorbed Pb and Pb-INC = incorporated Pb.

(Schwertmann and Murad, 1983), therefore the incorporation of Pb is likely linked to this process. We suggest that as the goethite particles are growing, Pb adsorbed onto surfaces becomes incorporated as crystal growth occurs. This is consistent with our observations, as the main phase of Pb incorporation i.e. within first 24 h, is coincident with the goethite crystallization reaction (Figs. 4 and 8). The amount of Pb incorporated into goethite at pH 13 and 21 °C was larger than that incorporated in hematite/goethite formed at pH 5 and 92 °C (~50% compared to ~20%, Figs. 6 and 8, Supplementary material Fig. S8). This higher uptake is likely to be due to both the differences in crystallization mechanisms between hematite and goethite, and because goethite has a higher capacity for incorporating foreign cations compared to hematite (Cornell and Schwertmann, 2003; and references therein). The goethite crystallization reaction allows Pb incorporation throughout the entire crystal growth process with Pb constantly incorporated into the growing crystals. There is no indication that Pb is expelled from the goethite during later stages of crystallization (incorporated Pb is virtually constant after 24 h, Fig. 8), suggesting that any Pb incorporated in goethite may be non-labile in the long term.

3.3. Unit cell size analysis

The unit cell dimensions of the end-product hematite (pH 5) and goethite (pH 13) samples crystallized in the presence of Pb were mostly within error of those for pure hematite or goethite synthesized at the same conditions (Table 1). Close examination of the data indicates that the hematite *c* axis length and the goethite *b* axis length show an increase above the error of the analysis. However, the increase is very small, and due to the lack of consistency of this increase in all dimensions of each phase, we

Table 1
Unit cell parameters (in Å) for hematite and goethite samples, and uncertainties (2σ, in Å) from calculation using the Unitcell program (Holland and Redfern, 1997); Δ_x (in Å) represents the difference in the unit cell parameters between the hematite/goethite end-products in the presence of Pb, and pure hematite/goethite that was synthesized at the same conditions.

Sample	*a* Axis	Δ_a	$2\sigma_a$	*b* Axis	Δ_b	$2\sigma_b$	*c* Axis	Δ_c	$2\sigma_c$
Hematite (end-product, −Pb) after 5 days	5.03492	–	0.00052	–	–	–	13.73176	–	0.00366
Hematite (end-product, +Pb) after 5 days	5.03453	−0.0004	0.00052	–	–	–	13.74450	+0.01274	0.00368
Hematite$\left(\text{end}-\text{product},+\text{Pb}+\text{SO}_4^{2-}\right)$ after 5 days	5.03414	−0.0008	0.00052	–	–	–	13.74982	+0.01806	0.00368
Goethite (end-product, −Pb) after 5 days	4.61311	–	0.00174	9.94365	–	0.0019	3.02272	–	0.00038
Goethite (end-product, +Pb) after 5 days	4.61652	+0.00341	0.00174	9.95224	+0.00859	0.0019	3.02234	−0.00038	0.00038

consider these to be negligible. Previous studies show that when large cations (e.g. Cd^{2+}) substitute directly for Fe^{3+} in the goethite structure this leads to an increase in unit cell dimensions. For example, substitution of Cd^{2+} (ionic radius = 0.95 Å) at 0.99 mol% (Cd /(Fe + Cd) * 100)) produced an increase of 0.0115, 0.0037 and 0.0053 Å, in the *a*, *b* and *c* axis dimensions of goethite, respectively (Sileo et al., 2003). Also, Larralde et al. (2012) reported that Sn^{2+} (ionic radius of 1.18 Å) substitution into goethite structure at 2.1 mol% led to increases in the *a*, *b* and *c* axis dimensions of 0.0157, 0.0037 and 0.0012 Å, respectively. This indicates that if the Pb^{2+} in this study was directly substituting for Fe^{3+} it would lead to an increase in all unit cell dimensions for goethite and/or hematite. The unit cell results suggest that the Pb in both systems (pH 5 and 13) is not directly substituted for Fe^{3+} in the structures of hematite or goethite. This is not surprising as the ionic radius of Pb^{2+} is almost double that of Fe^{3+} (i.e. 0.643 Å Fe^{3+} vs. 1.19 Å Pb^{2+}). This make Pb^{2+} highly incompatible within the structure of hematite or goethite, as usually only small differences in ionic radii are tolerated for direct substitution to occur (<±18% difference in ionic radii, Cornell and Schwertmann, 2003).

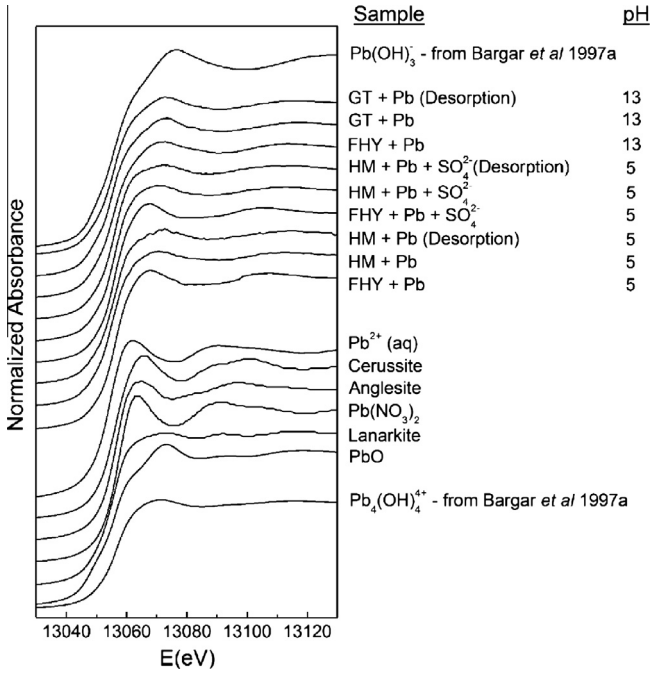

Fig. 9. Normalized Pb X-ray Absorption Near Edge Structure spectra from the ferrihydrite starting materials, end-products of the ferrihydrite crystallization experiments, and standard phases. E_o for Pb L_{III} edge is at 13,055 eV. FHY = ferrihydrite (starting materials), GT = goethite (end-product of the transformations) and HM = hematite (end-product of the transformations). Desorption samples had surface adsorbed Pb removed.

3.4. XAS results and discussion

3.4.1. Pb-L_{III} edge X-ray Absorption Near Edge Structure (XANES) analysis

Comparison of the size, shape and position of the peaks in the Pb-XANES spectra of experimental samples and standards (Fig. 9) indicated that none of the Pb-XANES spectra from the standards matched those of the experimental samples. It is, therefore, likely that Pb precipitates were absent in the experimental samples. This finding is consistent with our modelling results which predicted that all solutions were undersaturated with respect to solid Pb phases (Supplementary material, Fig. S1 and text).

XANES spectra from samples at pH 5, including the desorption samples, had a broad peak centred on approximately 13,070 eV and a second broad maximum between 13,104 and 13,115 eV. These peaks are broader and centred at slightly higher energy (3–8 eV) compared to the peaks in the spectra from the initial Pb-ferrihydrite. All the spectra from the pH 5 samples were very similar to spectra of $Pb_4(OH)_4^{4+}$ (aq) from Bargar et al. (1997a) (Pb with distorted trigonal pyramid configuration). This indicates that, consistent with previous studies, the Pb formed inner sphere adsorption complexes on the iron (oxyhydr)oxides (e.g. ferrihydrite) surface with a similar coordination environments to $Pb_4(OH)_4^{4+}$ (aq) (Bargar et al., 1997b; Ostergren et al., 2000a,b; Trivedi et al., 2003).

XANES spectra from all the samples at pH 13 had maxima centred at approximately 13,075 and 13,120 eV. These XANES spectra compare well to the Pb XANES spectra of $Pb(OH)_3^-$ (aq) (Pb with undistorted trigonal pyramid configuration, Bargar et al., 1997b). This is consistent with the fact that at pH 13.5 > 99% of Pb^{2+} in solution is present as $Pb(OH)_3^-$ (aq) (Baes and Messmer, 1976). We suggest that this is indicative of inner sphere adsorption of Pb to the goethite surface.

3.4.2. Extended X-ray Absorption Fine Structure (EXAFS) analysis

Fig. 10 shows the k^3 weighted Pb-EXAFS and their Fourier transforms for all the analyzed samples. The results from the fits of the EXAFS are presented in Table 2.

Fitting the EXAFS spectra revealed that the first shell of atoms surrounding the Pb in all samples consisted of 2–3 oxygen atoms at distances ranging from 2.27 to 2.37 Å. A second shell of iron atoms with a coordination number of 0.8–1.6 with bond distances ranging from 3.30 to 3.36 Å was also fitted to the EXAFS spectra from the starting material (i.e., Pb adsorbed to ferrihydrite at pH 5 and 13), but could not be fitted to the data from the crystalline end-products.

The bond lengths and coordination numbers for Pb adsorbed to ferrihydrite at pH 5 and 13 are consistent with previously studies of Pb adsorption to ferrihydrite at neutral to slightly acidic conditions (i.e., pH 4.5–7, Bargar et al., 1998; Ostergren et al., 2000a,b; Trivedi et al., 2003), although minor differences are evident. Firstly, the first shell oxygen bond distances (2.29–2.35 Å) are slightly larger than the reported values (2.27–2.32 Å) for Pb adsorption to iron

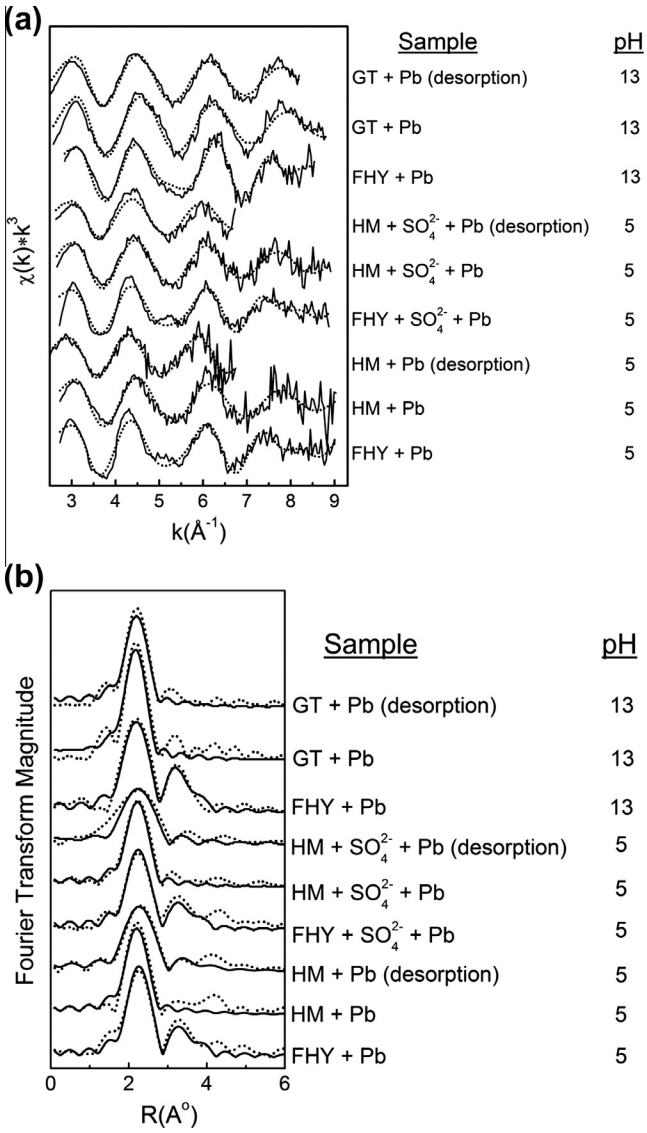

Fig. 10. (a) Pb EXAFS from starting materials and end-products of the ferrihydrite crystallization experiments and (b) the corresponding Fourier transform plots (dotted curves are fits to the data). FHY = ferrihydrite (starting materials), GT = goethite (end-product of the transformations) and HM = hematite (end-product of the transformations). Desorption samples had surface adsorbed Pb removed.

(oxyhydr)oxides (Bargar et al., 1997a,b; Elzinga et al., 2001; Ostergren et al., 2000a; Trivedi et al., 2003; Weesner and Bleam, 1998) but within error of first shell bond distances of Pb adsorbed to aluminium oxides (Bargar et al., 1997a). The difference in the Pb–O bond distances between ours and previous studies could stem from the difference in the temperatures at which the Pb-XAS data were collected. The spectra in the current study were collected at liquid nitrogen temperature (77 K), whereas the spectra in the previous works were collected at room temperature (Bargar et al., 1997a,b; Elzinga et al., 2001; Ostergren et al., 2000a,b; Rouff et al., 2004; Strawn and Sparks, 1999; Trivedi et al., 2003). Bargar et al. (1997a) has shown that freezing condition caused changes in the Pb bonding environment, leading to more distant O in the first shells being distinguished leading to longer apparent bond distances. Secondly, the coordination numbers of the 2nd shell of iron atoms is ~1 lower than those reported by Trivedi et al. (2003) for Pb adsorption to ferrihydrite at near neutral pH (CN ~2). However, the errors on the coordination numbers determined from EXAFS analysis are relatively large (±1), therefore we suggest that the values calculated in this study are within error of those previously reported. This indicates that, consistent with previous studies, Pb was adsorbed to ferrihydrite via a bidentate mononuclear inner sphere adsorption complex. This also indicates that the adsorption mechanism of Pb to ferrihydrite does not change from neutral pH to pH 13. The data also clearly showed no difference in bonding environment between the samples with and without SO_4^{2-} at equivalent pH. This is consistent with observations from Ostergren et al. (2000a) who also observed that the Pb–O bond lengths and adsorption mechanism (inner sphere either edge sharing or corner sharing complexes) were unaffected by the presence of SO_4^{2-}.

The first oxygen shell bond distances and coordination numbers of the Pb associated with the crystalline end-products were very similar to those of Pb adsorbed to ferrihydrite. However, the lack of a second shell in the Pb EXAFS data from the end-product samples suggests that the Pb coordination environment has changed in some way during the crystallization reaction. The chemical extraction data indicate that approximately 20–50% of the total Pb was incorporated while 40% to ~60% of the total Pb remained surface bound. Thus, the EXAFS signal of the end-products was a composite of the Pb in a number of different coordination environments. Data from the desorbed samples, which had most surface bound Pb removed, did not show a significant second shell either. However, the concentration of Pb is 50–60% lower in the desorption samples compared to the starting materials. This could account for the poor quality of the data at $k > 6$ Å^{-1} which constrained the ability to fit a second shell to these EXAFS data. This data indicates that Pb was not substituting for Fe within the crystalline lattice as this would likely lead to a large coordination number in the second shell due to the presence of Fe backscatters at fixed geometry and bond distances. It is more likely that Pb is present within non-crystallographic site e.g., defects or nanopores, within the hematite/goethite crystals. This is consistent with the unit cell size

Table 2
Pb-EXAFS fitting results for ferrihydrite adsorption samples (starting materials) and the end-products of ferrihydrite crystallization at pH 5 and pH 13. CN is coordination number, R is interatomic distance (Å) and $2\sigma^2$ is the Debye Waller factor (Å^2). Debye Waller factors were fixed at 0.02. Desorption samples had surface adsorbed Pb removed.

Sample	pH	Description	Bond type	CN	R (Å)	R factor	$2\sigma^2$ (Å^2)
FHY + Pb	5	Ferrihydrite with Pb, adsorption for 24 h	Pb–O	2.5	2.35	57.9	0.02
			Pb–Fe	0.9	3.35	51.4	0.02
HM + Pb	5	Hematite and goethite with Pb, after transformation	Pb–O	2.2	2.31	48.8	0.02
HM + Pb (desorption)	5	Hematite and goethite with Pb, after desorption	Pb–O	1.9	2.37	48.2	0.02
FHY + Pb + SO_4^{2-}	5	Ferrihydrite with Pb and SO_4^{2-}, adsorption for 24 h	Pb–O	2.2	2.35	50.3	0.02
			Pb–Fe	0.8	3.36	44.6	0.02
HM + Pb + SO_4^{2-}	5	Hematite and goethite with Pb and SO_4^{2-}, after transformation	Pb–O	2.2	2.33	42.3	0.02
HM + Pb + SO_4^{2-} (desorption)	5	Hematite and goethite with Pb and SO_4^{2-}, after desorption	Pb–O	1.9	2.36	41.8	0.02
FHY + Pb	13	Ferrihydrite with Pb, adsorption for 30 min	Pb–O	2.5	2.29	43.9	0.02
			Pb–Fe	1.6	3.30	29.3	0.02
GT + Pb	13	Goethite with Pb, after transformation	Pb–O	2.8	2.27	38.5	0.02
GT + Pb (desorption)	13	Goethite with Pb, after desorption	Pb–O	2.3	2.30	34.1	0.02

analysis which also indicated a lack of direct substitution of Pb^{2+} for Fe^{3+} within the iron (oxyhydr)oxide structure.

4. Pb incorporation mechanism into hematite and goethite, and implications for natural and contaminated environments

This study, in conjunction with our previous work (Vu et al., 2010), shows that during the crystallization of hematite and goethite from Pb-adsorbed ferrihydrite a significant proportion (between 20% and 70%) of the initially adsorbed Pb becomes incorporated into hematite or goethite particles. At the lower temperatures of the current study, the amount of adsorbed Pb incorporated into hematite (~20%) is much less than at high temperatures (~70%, Vu et al., 2010). However, the mechanism of Pb incorporation was the same i.e., rapid incorporation of the adsorbed Pb prior to the main crystallization phase. The EXAFS and unit cell analyses indicate that the Pb is substituted into a non-crystallographic site within the iron oxide lattice, possibly within defects. This is supported by the fact that Pb is expelled from the hematite during crystallization, suggesting that the incorporated Pb is incompatible with the crystalline structures, and is therefore released as the crystallinity increases and defect density decreases. However, in natural systems where the incorporated concentration of Pb is likely to be significantly lower, the proportion of Pb released during crystallization may be much less, as a lower concentration of defect sites will be required. The incorporation of Pb into goethite at ambient conditions and high pH occurs via absorption of Pb as the goethite crystals grow, leading to a more gradual uptake over the entire crystallization process when compared to hematite. The XAS and unit cell data for Pb substitution into goethite indicate that, similar to hematite, the Pb is taken up into a non-crystallographic site without affecting the bulk structure. However, there was a lack of Pb rerelease during the later stages of crystallization indicating that goethite may be better at retaining Pb relative to hematite. This may be due to goethite having a higher capacity for incorporating foreign cations or due to the change in Pb coordination environment between near neutral and alkaline pH (i.e., the undistorted trigonal pyramid coordination of Pb at pH 13 may be more easily accommodated than the distorted trigonal pyramid coordination at pH 5). However, without further information no further conclusions can be drawn. It should be noted that the rate of iron (oxyhydr)oxide crystallization may be significantly slower in natural systems compared to the experiments in this study, due to lower temperatures and the effect of foreign ions. This may lead to a significant decrease in the proportion of adsorbed Pb incorporated during crystallization.

The results from this study highlight that crystallization and crystal growth of iron (oxyhydr)oxides are the keys to Pb incorporation. Adsorbed Pb could become incorporated into goethite and hematite in natural or anthropogenic environments where these phases are actively forming or crystallizing. This includes several key natural systems. For example, during weathering of iron bearing silicate minerals (Banfield and Eggleton, 1988), iron (oxyhydr)oxides are formed during soil formation. A proportion of adsorbed Pb present within this environment is likely to become incorporated into the iron (oxyhydr)oxide particles. This can also explain the reason for the significant link between Pb and Fe concentrations in soils and within fresh water colloids (e.g., in rivers, Hassellov and von der Kammer, 2008; Kaste et al., 2006). Due to the nanoparticulate size of these particles they can then be transported within rivers as colloidal particles for very long periods (years) and distances (up to hundreds of kilometres, Gustafsson et al., 2000; Kimball et al., 1995). The non-labile nature of the incorporated Pb means that within fresh water systems the Pb will not be dissociated. Lead can only be released from the solid if the iron (oxyhydr)oxide particles are dissolved, which can only occur at extremely acidic pH's (1–2) or during reductive dissolution e.g., if the colloids are buried within anaerobic sediments. However, during normal riverine conditions this is very unlikely implying that Pb could be transported over great distances into the marine environment via this transport vector.

The incorporation of Pb into iron (oxyhydr)oxide phases is also important for contaminated land systems, for example Pb is strongly associated with these phases in acid mine drainage environments (Hudson-Edwards et al., 1999; Kimball et al., 1995). Finally, ^{210}Pb is a significant long-term risk for geological disposal of radioactive waste. Interaction of ^{210}Pb with iron (oxyhydr)oxides in this system could lead to significant immobilization of ^{210}Pb within and/or close to the repository, limiting its transport to colloidal migration only.

Acknowledgements

This work was funded by a Dorothy Hodgkin Postgraduate Award (HPV) and UK CCRLC award for beamtime (46304) to LGB. We thank Bob Bilsborrow and John Charnock from, Daresbury Laboratory for their help with collecting and interpreting the XAS data. Fred Mosselmans from Diamond Light Source Ltd is acknowledged for helpful comments. Andrew Brown and Steeve Bonneville from the University of Leeds are thanked for their help in the TEM imaging.

Appendix A. Supplementary material

Supplementary data associated with this article can be found, in the online version, at http://dx.doi.org/10.1016/j.apgeochem.2013.10.001.

References

Baes, C.F., Messmer, R.E., 1976. The Hydrolysis of Cations. John Willey & Sons Inc., New York.
Baltpurvins, K.A., Burns, R.C., Lawrance, G.A., Stuart, A.D., 1996. Effect of pH and anion type on the aging of freshly precipitated iron(III) hydroxide sludges. Environmental Science and Technology 30, 939–944.
Baltpurvins, K.A., Burns, R.C., Lawrance, G.A., Stuart, A.D., 1997. Effect of Ca^{2+}, Mg^{2+}, and anion type on the aging of iron(III) hydroxide precipitates. Environmental Science and Technology 31, 1024–1032.
Banfield, J.F., Eggleton, R.A., 1988. Transmission electron-microscope study of biotite weathering. Clays and Clay Minerals 36, 47–60.
Bargar, J.R., Brown, G.E., Parks, G.A., 1997a. Surface complexation of Pb(II) at oxide–water interfaces. 1. XAFS and bond-valence determination of mononuclear and polynuclear Pb(II) sorption products on aluminum oxides. Geochimica et Cosmochimica Acta 61, 2617–2637.
Bargar, J.R., Brown, G.E., Parks, G.A., 1997b. Surface complexation of Pb(II) at oxide-water interfaces. 2. XAFS and bond-valence determination of mononuclear Pb(II) sorption products and surface functional groups on iron oxides. Geochimica et Cosmochimica Acta 61, 2639–2652.
Bargar, J.R., Brown, G.E., Parks, G.A., 1998. Surface complexation of Pb(II) at oxide–water interfaces: III. XAFS determination of Pb(II) and Pb(II)-chloro adsorption complexes on goethite and alumina. Geochimica et Cosmochimica Acta 62, 193–207.
Bethke, C.M., 2004. GWB Reference Manual, The Geochemist's Workbench® Release, 5.0 ed. Hydrogeology Program, University of Illinois.
Binsted, N., 1998. EXCURV98: CCLRC Daresbury Laboratory Computer Program.
Bruker, 2009. Diffrac Plus – Topas 4.2 Tutorial, Karlsruhe, Germany.
Collins, C.R., Ragnarsdottir, K.V., Sherman, D.M., 1999. Effect of inorganic and organic ligands on the mechanism of cadmium sorption to goethite. Geochimica et Cosmochimica Acta 63, 2989–3002.
Combes, J.M., Manceau, A., Calas, G., 1990. Formation of ferric oxides from aqueous-solutions – a polyhedral approach by X-ray absorption-spectroscopy. 2. Hematite formation from ferric gels. Geochimica et Cosmochimica Acta 54, 1083–1091.
Cornell, R.M., Giovanoli, R., 1985. Effect of solution conditions on the proportion and morphology of goethite formed from ferrihydrite. Clays and Clay Minerals 33, 424–432.
Cornell, R.M., Schwertmann, U., 2003. The Iron Oxides: Structure, Properties, Reactions, Occurrences and Uses. Wiley-VCH, Weinheim.

Davidson, L.E., Shaw, S., Benning, L.G., 2008. The kinetics and mechanisms of schwertmannite transformation to goethite and hematite under alkaline conditions. American Mineralogist 93, 1326–1337.
Elzinga, E.J., Peak, D., Sparks, D.L., 2001. Spectroscopic studies of Pb(II)–sulfate interactions at the goethite–water interface. Geochimica et Cosmochimica Acta 65, 2219–2230.
Fischer, W.R., Schwertmann, U., 1975. Formation of hematite from amorphous iron(III) hydroxide. Clays and Clay Minerals 23, 33–37.
Ford, R.G., Bertsch, P.M., Farley, K.J., 1997. Changes in transition and heavy metal partitioning during hydrous iron oxide aging. Environmental Science and Technology 31, 2028–2033.
Ford, R.G., Kemner, K.M., Bertsch, P.M., 1999. Influence of sorbate–sorbent interactions on the crystallization kinetics of nickel- and lead-ferrihydrite coprecipitates. Geochimica et Cosmochimica Acta 63, 39–48.
Gustafsson, O., Widerlund, A., Andersson, P.S., Ingri, J., Roos, P., Ledin, A., 2000. Colloid dynamics and transport of major elements through a boreal river – brackish bay mixing zone. Marine Chemistry 71, 1–21.
Hassellov, M., von der Kammer, F., 2008. Iron oxides as geochemical nanovectors for metal transport in soil–river systems. Elements 4, 401–406.
Holland, T.J.B., Redfern, S.A.T., 1997. Unit cell refinement from powder diffraction data: the use of regression diagnostics. Mineralogical Magazine 61, 65–77.
Hudson-Edwards, K.A., Schell, C., Macklin, M.G., 1999. Mineralogy and geochemistry of alluvium contaminated by metal mining in the Rio Tinto area, southwest Spain. Applied Geochemistry 14, 1015–1030.
Jang, J.H., Dempsey, B.A., Catchen, G.L., Burgos, W.D., 2003. Effects of Zn(II), Cu(II), Mn(II), Fe(II), NO^{3-}, or SO_4^{2-} at pH 6.5 and 8.5 on transformations of hydrous ferric oxide (HFO) as evidenced by Mossbauer spectroscopy. Colloids and Surfaces A – Physicochemical and Engineering Aspects 221, 55–68.
Kaste, J.M., Bostick, B.C., Friedland, A.J., Schroth, A.W., Siccama, T.G., 2006. Fate and speciation of gasoline-derived lead in organic horizons of the northeastern USA. Soil Science Society of America Journal 70, 1688–1698.
Kimball, B.A., Callender, E., Axtmann, E.V., 1995. Effects of colloids on metal transport in a river receiving acid–mine drainage, upper Arkansas river, Colorado, USA. Applied Geochemistry 10, 285–306.
Kparmwang, T., 2003. Zinc adsorption and desorption at low concentrations by basaltic soil on Jos Plateau, Nigeria. Communications in Soil Science and Plant Analysis 34, 1589–1609.
Larralde, A.L., Ramos, C.P., Arcondo, B., Tufo, A.E., Saragovi, C., Sileo, E.E., 2012. Structural properties and hyperfine characterization of Sn-substituted goethites. Materials Chemistry and Physics 133, 735–740.
Li, Y.H., Di, Z.C., Ding, J., Wu, D.H., Luan, Z.K., Zhu, Y.Q., 2005. Adsorption thermodynamic, kinetic and desorption studies of Pb^{2+} on carbon nanotubes. Water Research 39, 605–609.
Lin, X.M., Burns, R.C., Lawrance, G.A., 2003. Effect of cadmium(II) and anion type on the ageing of ferrihydrite and its subsequent leaching under neutral and alkaline conditions. Water, Air, and Soil pollution 143, 155–177.
Loan, M., Newman, O.M.G., Farrow, J.B., Parkinson, G.M., 2006. Continuous reactive crystallization of nanoscale six-line ferrihydrite. Crystal Growth & Design 6, 79–86.
Loan, M., Newman, O.G.M., Farrow, J.B., Parkinson, G.M., 2008. Effect of rate of crystallization on the continuous reactive crystallization of nanoscale 6-line ferrihydrite. Crystal Growth & Design 8, 1384–1389.
Martinez, C.E., McBride, M.B., 1998a. Coprecipitates of Cd, Cu, Pb and Zn in iron oxides: solid phase transformation and metal solubility after aging and thermal treatment. Clays and Clay Minerals 46, 537–545.
Martinez, C.E., McBride, M.B., 1998b. Solubility of Cd^{2+}, Cu^{2+}, Pb^{2+}, and Zn^{2+} monitored in aged coprecipitates with amorphous iron hydroxides. Environmental Science and Technology 32, 743–748.
Martinez, C.E., Sauve, S., Jacobson, A., McBride, M.B., 1999. Thermally induced release of adsorbed Pb upon aging ferrihydrite and soil oxides. Environmental Science and Technology 33, 2016–2020.
Murray, J., Kirwan, L., Loan, M., Hodnett, B.K., 2009. In-situ synchrotron diffraction study of the hydrothermal transformation of goethite to hematite in sodium aluminate solutions. Hydrometallurgy 95, 239–246.
Ostergren, J.D., Brown, J.G.E., Parks, G.A., Persson, P., 2000a. Inorganic ligand effects on Pb(II) sorption to goethite ([alpha]-FeOOH): II. Sulfate. Journal of Colloid and Interface Science 225, 483–493.
Ostergren, J.D., Trainor, T.P., Bargar, J.R., Brown, G.E., Parks, G.A., 2000b. Inorganic ligand effects on Pb(II) sorption to goethite (alpha-FeOOH) – I. Carbonate. Journal of Colloid and Interface Science 225, 466–482.
Rouff, A.A., Elzinga, E.J., Reeder, R.J., Fisher, N.S., 2004. X-ray absorption spectroscopic evidence for the formation of Pb(II) inner-sphere adsorption complexes and precipitates at the calcite–water interface. Environmental Science and Technology 38, 1700–1707.
Schwertmann, U., Murad, E., 1983. Effect of pH on the formation of goethite and hematite from ferrihydrite. Clays and Clay Minerals 31, 277–284.
Schwertmann, U., Friedl, J., Stanjek, H., 1999. From Fe(III) ions to ferrihydrite and then to hematite. Journal of Colloid and Interface Science 209, 215–223.
Schwertmann, U., Stanjek, H., Becher, H.H., 2004. Long-term in vitro transformation of 2-line ferrihydrite to goethite/hematite at 4, 10, 15 and 25 degrees C. Clay Minerals 39, 433–438.
Shaw, S., Pepper, S.E., Bryan, N.D., Livens, F.R., 2005. The kinetics and mechanisms of goethite and hematite crystallization under alkaline conditions, and in the presence of phosphate. American Mineralogist 90, 1852–1860.
Sileo, E.E., Solis, P.S., Paiva-Santos, C.O., 2003. Structural study of a series of synthetic goethites obtained in aqueous solutions containing cadmium(II) ions. Powder Diffraction 18, 50–55.
Strawn, D.G., Sparks, D.L., 1999. The use of XAFS to distinguish between inner- and outer-sphere lead adsorption complexes on montmorillonite. Journal of Colloid and Interface Science 216, 257–269.
Swedlund, P.J., Webster, J.G., Miskelly, G.M., 2003. The effect of SO_4 on the ferrihydrite adsorption of Co, Pb and Cd: ternary complexes and site heterogeneity. Applied Geochemistry 18, 1671–1689.
Trivedi, P., Dyer, J.A., Sparks, D.L., 2003. Lead sorption onto ferrihydrite. 1. A macroscopic and spectroscopic assessment. Environmental Science and Technology 37, 908–914.
Viollier, E., Inglett, P.W., Hunter, K., Roychoudhury, A.N., Van Cappellen, P., 2000. The ferrozine method revisited: Fe(II)/Fe(III) determination in natural waters. Applied Geochemistry 15, 785–790.
Vu, H.P., Shaw, S., Brinza, L., Benning, L.G., 2010. Crystallization of hematite (alpha-Fe(2)O(3)) under alkaline condition: the effects of Pb. Crystal Growth & Design 10, 1544–1551.
Weesner, F.J., Bleam, W.F., 1998. Binding characteristics of Pb^{2+} on anion-modified and pristine hydrous oxide surfaces studied by electrophoretic mobility and X-ray absorption spectroscopy. Journal of Colloid and Interface Science 205, 380–389.
Yuwono, V.M., Burrows, N.D., Soltis, J.A., Do, T.A., Penn, R.L., 2012. Aggregation of ferrihydrite nanoparticles in aqueous systems. Faraday Discussions 159, 235–245.